Journal of the Korean Physical Society, Vol. 44, No. 2, February 2004, pp. 435∼441

Application of a Rocket-Borne UV Radiometer Onboard KSR-III for O_3 Measurements

Seung-Hyun Hwang, Soo-Jin Lee, Jun-Kyu Kim, Young-Soon Jang, Jeong-Joo Park and Gwang-Rae Cho
Korea Space Launch Vehicle Program Office, Korea Aerospace Research Institute, Daejeon 305-333

Jhoon Kim* and Hi Ku Cho
Global Environment Laboratory, Department of Atmospheric Science, Yonsei University, Seoul 120-749

Seung-Hoon Lee
Satellite Application Department, Korea Aerospace Research Institute, Daejeon 305-333

Young In Won
Polar Science Laboratory, Korea Ocean R&D Institute, Ansan 426-744

(Received 11 March 2003, in final form 5 January 2004)

KSR-III, the third Korean Sounding Rocket, was launched successfully at Anheung, Korea on Nov. 28, 2002. One of the scientific missions of KSR-III was to measure the stratospheric ozone density profile by using an onboard four-channel UV radiometer. The apogee of the rocket was 42.8 km, and the total flight time was 231 s. The UV radiometer onboard the KSR-III measured the attenuation of solar radiation during ascending phase to obtain a vertical profile of the ozone density. The detector has UV channels centered at 255, 290, and 310 nm and a visible channel at 450 nm for attitude reference. Because the measurement of the solar radiation depends on the response function of the sensor, calibrations of interference filters and phototubes must be done. The optical calibration system consists of a monochromator, an optical power meter, light detectors, standard light sources, a control PC, and data acquisition software. The application of the rocket-borne UV radiometer onboard the KSR-III to the ozone measurement are presented together with the calibration results from the integrated calibration system at the Korea Aerospace Research Institute. Using the calibration results and the *in-situ* measurement data, we obtained the ozone number density profile, and compared with other measurements.

PACS numbers: 93.07, 97.42, 97.92
Keywords: Sounding rocket, UV radiometer, Ozone density, Calibration

I. INTRODUCTION

Various methods exist to measure the vertical ozone density profile in the atmosphere. Ground-based instruments, balloons, aircraft, sounding rockets, and satellites have been used as platforms to measure the ozone density profile. Balloon cannot give accurate information above a 30-km altitude due to their bursting, and satellites have an altitude limit in orbit, so rocket-borne measurements using a radiometer is a unique *in-situ* method to measure the middle atmospheric ozone density profile. Balloon-borne observations have been gradually decreasing for decades, but studies on the detailed mechanisms of the upper troposphere and the lower stratosphere by various balloon programs are still being carried out actively [1–4].

The most famous rocket-borne instrument is the ROCOZ (Rocket Ozonesonde) radiometer [5]. Several rocket soundings have been performed using optical ozonesondes [6]. The satellite-based observations have been increasing over the past 25 years, and recent well-known satellite missions for ozone measurements are the GOME (Global Ozone Monitoring Experiment), the SAGE (Stratospheric Aerosol and Gas Experiment), the POAM (Polar Ozone and Aerosol Measurement), the HALOE (HALogen Occultation Experiment), the GOMOS (Global Ozone Monitoring by Occultation of Stars), and MSX/UVISI (Midcourse Space Experiment/Ultraviolet and Visible Imagers and Spectrographic Imagers) [7–11]. With these missions, numerous studies, including the three-dimensional ozone distribution and even long-term trend analysis, are actively

*E-mail: jkim2@yonsei.ac.kr; Fax: +82-2-365-5163

in progress. The KSR (Korea Sounding Rocket) series, which was first launched in June 4, 1993, obtained several sounding data on ozone concentration profiles in the middle atmosphere over the Korean Peninsula [12,13].

Recently, KSR-III was launched successfully on Nov. 28, 2002 reaching an apogee of 42.8 km. The engineering goal of KSR-III was to evaluate the Korea's first liquid propulsion engine system. For the scientific mission, four-channel radiometers were onboard the rocket: three UV channels centered at 255 ± 15, 290 ± 15, and 310 ± 15 nm detect direct solar UV radiation and a visible channel at 450 ± 3 nm to detect the angular change of the rocket for each UV channel during the ascending phase. To retrieve the ozone slant column density, one has to obtain the radiometer response function, which is the product of the interference filter and the phototube before the flight. The calibration system at the Optical Laboratory of the Korea Aerospace Research Institute (KARI) was used to verify and calibrate the performance of the radiometer. The calibration system consists of a monochromator, light sources, detectors, an optical power meter (OPM), a control PC, and data acquisition software.

In this paper the development of the UV radiometer onboard the KSR-III and the comparison of the calibration results with the manufacturer's values are presented. Using these results and the measured solar UV intensity from the flight tests, the vertical ozone number density profile over the Korean Peninsula was retrieved and showed reasonable agreement with other observations in the lower stratosphere.

II. PRINCIPLE

The ozone absorbs the solar UV radiation in the Huggins and Hartley band at UV wavelengths. This property of the solar radiation leads to the basic principle for a radiometer to detect ozone concentrations. If the attenuation of the solar radiation by the earth's atmosphere is assumed to be caused solely by ozone absorption and molecular scattering (ignoring aerosol scattering), the solar flux at altitude z is given by the Beer-Bouguer-Lambert law [14]:

$$I(z) = I(z_0)\exp[-\sigma_a N(z) - \sigma_s M(z)], \tag{1}$$

where $I(z)$ denotes the measured solar flux at an altitude z through a given interference filter, $I(z_0)$ is the incident solar intensity at the highest altitude (z_0) where the atmospheric density is negligible. $N(z)$ is the ozone column density at the observing height along the path between the instrument and the sun, and $M(z)$ is the slant-path air-column density at z. σ_a and σ_s are the effective ozone absorption and molecular scattering cross sections, respectively. Among the molecular scattering term, the Rayleigh scattering effect becomes dominant at the wavelengths considered in case of a clear sky [15]. Once σ_a is known, the ozone concentration can be calculated by introducing the measured solar flux ratio $I(z)/I(z_0)$ for a given altitude. The relationship between the measured solar flux ratio and the slant ozone column density is written as

$$\frac{I(z)}{I(z_0)} = \frac{\int_{\lambda_1}^{\lambda_2} F(\lambda)S(\lambda,\theta)\exp[-\sigma_a(\lambda,T(z))N(z) - \sigma_R(\lambda)M(z)]d\lambda}{\int_{\lambda_1}^{\lambda_2} F(\lambda)S(\lambda,\theta_0)d\lambda}, \tag{2}$$

where $F(\lambda)$ is the solar flux at the top of the atmosphere as a function of wavelength λ, $S(\lambda,\theta)$ is the response function of the radiometer calibrated in the laboratory, which is the product of the phototube response function, $S_{PT}(\lambda,\theta)$, and the interference filter response function, $S_{IF}(\lambda,\theta)$. θ is the incident angle between the sunlight and the detector pointing axis, and θ_0 is the measured value at the highest altitude, $\sigma_a(\lambda,T(z))$ is the absorption cross section as a function of wavelength and the temperature above z. $\sigma_R(\lambda)$ is the Rayleigh scattering coefficient. As long as the altitude of the highest rocket measurement (z_0) is far above the ozone peak at about 25 km, the absorption of ozone and the scattering effect of the atmosphere are negligible, and the exponential term in the denominator converges to zero as $N(z)$ and $M(z)$ become very small at $z = z_0$. However, if z_0 is not high enough to neglect the ozone absorption effect above z_0, Eq. (2) can be modified to take ozone absorption above $z = z_0$ into consideration [12]. Then, Eq. (2) can be written as

$$\frac{I(z)}{I(z_0)} = \frac{\int_{\lambda_1}^{\lambda_2} F(\lambda)S(\lambda,\theta)\exp[-\sigma_a(\lambda,T(z))N(z) - \sigma_R(\lambda)M(z)]d\lambda}{\int_{\lambda_1}^{\lambda_2} F(\lambda)S(\lambda,\theta_0)\exp[-\sigma_a(\lambda,T(z_0))N(z_0) - \sigma_R(\lambda)M(z_0)]d\lambda}, \tag{3}$$

where $N(z_0)$ and $M(z_0)$ are the ozone column density and the air column density at $z = z_0$.

If the solar flux intensity during the flight is obtained, the ozone column density can be calculated numerically

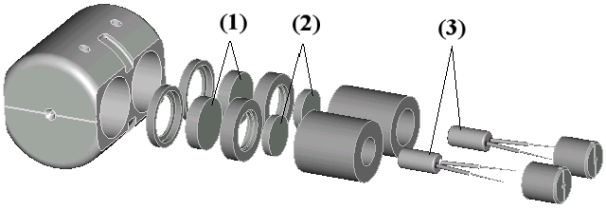

Fig. 1. Sensor parts configuration of one set: (1) quartz lens, (2) interference filters, (3) phototubes, and housings.

with the calibrated detector response functions. Then, the ozone number density can be retrieved by basically differentiating the column density obtained from Eq. (3) with respect to the altitude [12]. The validity of Eq. (3) was confirmed in the sensitivity tests of the retrieval to the selected $N(z_0)$ and $M(z_0)$. Enforced errors in $N(z_0)$ and $M(z_0)$ as large as 50 % were found to cause overall retrieval errors of less than 10 % and 0.5 %, respectively. The values of $N(z_0)$ and $M(z_0)$ are taken from climatological values, which are reasonable in most cases.

III. INSTRUMENTATION

The UV radiometer mainly consists of sensor parts and electronic circuit parts. A total of four sets of sensor parts are located at the inner skin of the electronic payload section. One set contains two channels: One detects the UV band radiation intensity and the other detects the visible band for an attitude reference. Each channel consists of a quartz lens, an interference filter, and a phototube. The configuration of the sensor part is shown in Fig. 1. The quartz lens (1), as an optical window, protects the filter head from possible disturbance during the flight and transmits the incoming solar radiation to the detector. The interference filter (2) transmits light in the specific wavelength range of interest. As a detector, the phototube (3) has a current response to light intensity. For the visible band, an R414 phototube (from Hamamatsu) and 450-nm interference filter are used, and an R840 phototube (from Hamamatsu) and UV interference filter are for UV bands. The main housing in the left part of Fig. 1 is made of aluminum, and other housings for optical parts are made of graphite teflon to protect from the thermal and the vibrational environments during the flight. All parts of the housings are designed and anodized in black to minimize the light reflection and scattering.

The electronic circuit parts have a pre-amplifier, a six step auto-gain circuit, an analog and gain output, and a telemetry system. The current output of the phototube is converted into the voltage in the pre-amplifier circuit. This voltage output is amplified in the six-step auto-gain circuit having 0, 4, 16, 64, 256, and 1024 gain steps. To compensate for the gain offset, we adopted an offset nulling circuit. The amplified analog output and

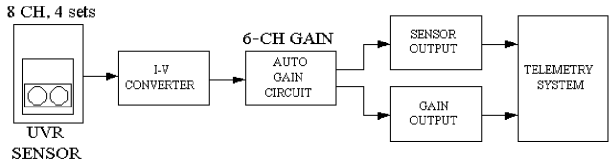

Fig. 2. Block diagram of the radiometer electronic parts.

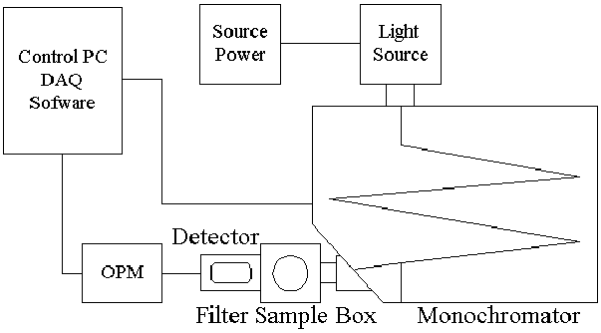

Fig. 3. Block diagram of the calibration system.

the gain are transmitted to the ground station through the telemetry system in the 0 ∼ 5-V range. The sampling rate of each channel is 200 samples/s with an 8-bit A/D converter. Figure 2 shows the block diagram of the electronic system [16]. Two channel of electronics are included in one PCB (Printed Circuit Board), and a total eight channels of electronics are integrated in four PCBs. The weight of the electronic system is 3 kg, including the circuit box.

The assigned DAM (data acquisition module) gathers and sends raw data to the TEU (telemetry encoder unit). The encoded data from the TEU are transmitted to the ground station through the onboard S-band transmitter. Transmitted data have a FM (frequency modulation) format, with PPL (Phase Locked Loop) structure. The telemetry data have 320 kbps PCM (Pulse Code Modulation) format and the modulated signal centered at 2.2 GHz is transmitted to the ground station in real-time [17].

IV. CALIBRATION

For the optical measurement system onboard satellites or rockets, such as ozone detectors, remote sensing instruments, sun sensors, and optical cameras, the optical filter and the detector must be calibrated before the flight tests.

The calibration of our radiometer system was performed at KARI's Optical Laboratory. Figure 3 shows the configured block diagram of the calibration system. The monochromator, ORIEL MS257, constitutes an important part of the calibration with monochromatic light discriminated in a 0.1-nm wavelength steps. The monochromatic light comes out through the axial

or lateral output port of the monochromator and penetrates into the sample filter. The light intensity from the monochromator has to be fixed to optimize the detector's response for our calibration by micromotor-driven adjustment of the slit mounted on the monochromator output port. The detector is mounted on the right behind of the sample filter box and directly measures the transmitted light intensity. These measured values are stored in the OPM. The monochromator and the OPM use the RS232 interface to communicate simultaneously with the control PC by using the serial port. The data acquisition software can control the monochromator grating, the wavelength range, and the OPM readout settings. The acquired data are saved in the control PC in an ASCII data file format.

To measure the filter response function, we must focus the monochromatic light source into the filter. The MS257 has a four-face grating turret with an automatic grating switching, and its stray light or re-entrant spectra is negligible and is suitable for measuring absorption, reflection, transmission, emission, and fluorescence of the sample from UV to IR (Infra-red) wavelength regions.

Mercury, D2 (Deuterium), and QTH lamps were employed in this system for light sources. The mercury lamp was used as a monochromator self-calibration light source. A 30-W D2 lamp was used as a calibration source in the UV region (185 $\sim$ 400 nm), and a 1-kW QTH lamp was used in the visible region. The QTH lamp has smooth spectral curve and stable output, so it is a useful light source to calibrate samples in the visible and the near-IR regions (300 $\sim$ 2500 nm). The D2 and the QTH lamp characteristics were measured first so that they could be used as spectral references for the calibration. Two detectors were used in this system. A UV-sensitive side-on type PMT (photo multiplier tube) was employed to detect the UV channel intensity, and a visible-sensitive photodiode silicon (Si) detector was employed to detect the visible channel intensity.

The monochromator scan range was about $\pm$50 nm from center wavelengths and the scan step was set to 0.2 nm for each test. Figure 4 shows the obtained response function curves for the four filters as the incident angle increased from 0° to 25° in 5° steps: (a) 255 nm, (b) 290 nm, (c) 310 nm, and (d) 450 nm. The manufacturer's center wavelength values and the test results for each filter at zero incident angle are compared in Table 1. The measured results have reasonable values within the maximum 1.2 % deviation.

One can calculate the angular response functions of each interference filter. Simple tilts in the incident light will cause the center wavelength to shift to a shorter wavelength. The following equation can be used to calculate the center wavelength shift for angles of incidence light up to 20° [18]:

$$\lambda_\theta = \lambda_0 \sqrt{1 - \left(\frac{n_0}{n^*}\right)^2 \sin^2\theta} \qquad (4)$$

where θ is the angle of incidence, λ_θ is the center wavelength at an incident angle of θ, λ_0 is the center wavelength at zero incident angle, n_0 is the refractive index of the medium surrounding the filter, normally it is 1 in air, and n^* is the effective refractive index of the filter specified as a numerical value derived for the indices of the thin film layers of the interference filter according to the composition of the filter (Table 2) [19]. Filters are made of UV fused silica material, so the effective refractive index of the filters is assumed as about 1.49, which was obtained from a linear interpolation of data in Table 2.

Figure 4 shows the response functions of each filter at six incident angles (0°, 5°, 10°, 15°, 20°, 25°) and confirms that each filter has its peak transmittance at its center wavelength. The center wavelength shifted to a

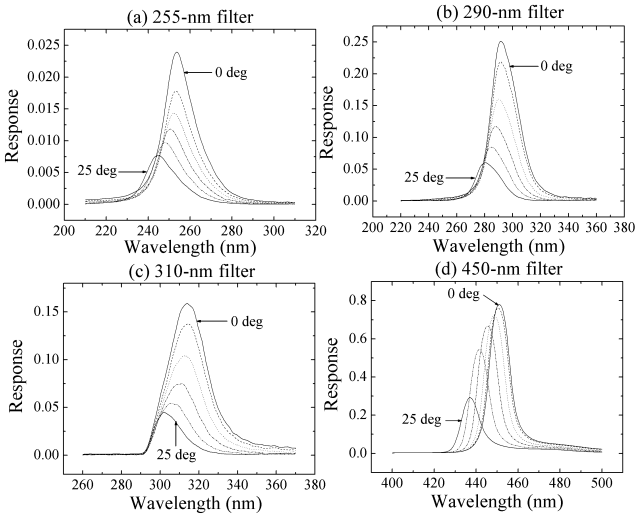

Fig. 4. Response function curves of each filter.

Table 1. Comparison of the center wavelength of each filter.

Filter	Manufacturer's	Measured
255 nm	252.9 nm	253.6 nm
290 nm	292.2 nm	291.6 nm
310 nm	310.2 nm	313.8 nm
450 nm	452.7 nm	452.0 nm

Table 2. Effective refractive index of the filter material for the given wavelengths.

Wavelength (nm)	UV Fused Silica
1060	1.450
643.8	1.457
587.6	1.458
546.1	1.460
486.1	1.463
346.6	1.477
248.2	1.509

Table 3. Comparison of the wavelength shifts for five incident angles.

Incident	255 nm		290 nm		310 nm		450 nm	
Angles	T*	E**	T	E	T	E	T	E
0°	252.9	253.6	292.2	291.6	310.2	313.8	452.7	452.0
5°	252.5	252.4	288.5	290.4	309.7	313.0	451.9	449.8
10°	251.2	250.6	287.0	287.8	308.1	311.0	449.6	446.6
15°	249.1	248.0	284.6	282.8	305.5	305.6	445.8	442.6
20°	246.1	244.6	281.3	280.4	301.9	302.0	440.6	438.0

*T: theoretical value, **E: empirical value

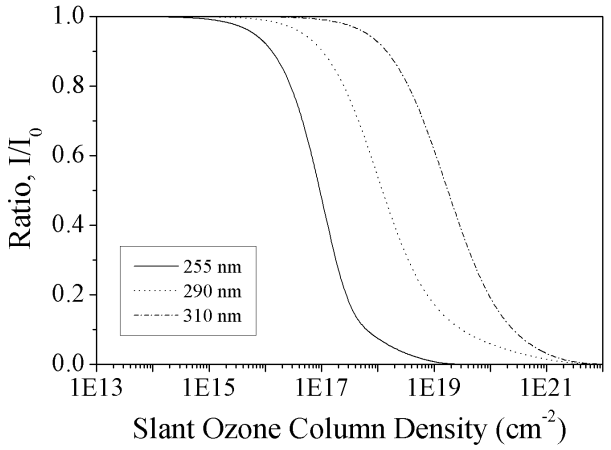

Fig. 5. Relationship between the intensity ratio (I/I_0) and the ozone column density.

shorter wavelength, and the lowered peak response trend was evaluated for each filter. Table 3 shows the comparison between the theoretical and the empirical values of the center wavelength shifts for the five incident angles. The R840 and R414 phototube response functions are taken from the Hamamastu datasheets [20]. A measurement of the angular response for the integrated radiometer was also carried out, and showed a typical cosine function response. The product of the response functions of the calibrated filter and the phototube is the radiometer response function and was used for the data reduction of the ozone column density for each channel as in the Eq. (3).

V. FLIGHT TESTS

The KSR-III was launched successfully on Nov. 28, 2002, from the west coast of the Korean peninsula (36°N, 136°E). The initial azimuth and elevation angle of the rocket at launch was 221° and 82.5°, respectively. The apogee of the rocket was 42.8 km, and the down-range distance was about 79.5 km. The UV radiometer measured the solar radiation during the ascending phase for a total flight time of 231 sec. The data reduction algo-

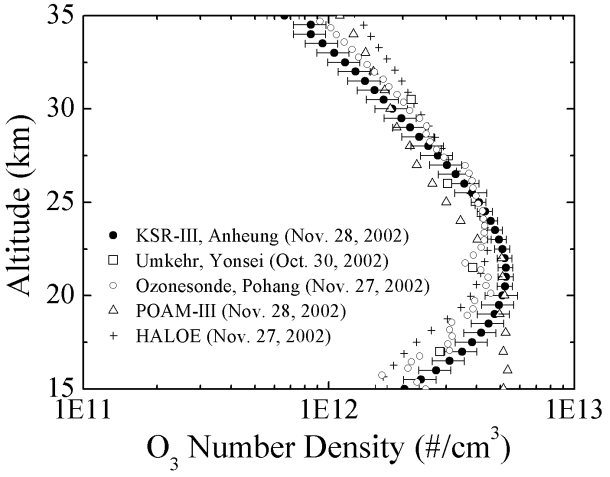

Fig. 6. Comparison of ozone density profiles from KSR-III with others.

rithm for obtaining the slant ozone column density was introduced in previous work [12]. With the calibration results, the relationship between the slant ozone column density (N) and the measured intensity ratio (I/I_0) for each channel was numerically obtained (Fig. 5). This relationship in Eq. (3) was calculated by using the solar flux from Mentall *et al.* [21] and Thekaekara [22], the absorption cross section from Molina and Molina [23], and the Rayleigh scattering cross sections from WMO [24]. From this relationship, the ozone column density was calculated at each channel and the ozone number density was retrieved by differentiating the column density with respect to the altitude considering sounding geometry.

The vertical ozone density profile over the Korean peninsula was obtained by using UV radiometer onboard the KSR-III and is shown in Fig. 6, which shows the retrieved density profile compared with the ground-based Dobson spectrophotometer (Umkehr measurements at Yonsei Univ., Seoul), ozonesonde (at KMA Pohang site), and satellite (HALOE onboard the UARS and POAM-III onboard the SPOT-4) measurements. Our results are in reasonable agreement with the others in the lower stratosphere, in general. The discrepancies tend to become large, especially for the HALOE measurements, for altitudes above the ozone density peak, which can be attributed to the attitude change of the rocket as it reaches apogee. Although all the compared measurements were not carried out at the same location, their data were taken over the Korean peninsula (near at 36°N, 126°E) except for the POAM-III instrument which passed at 60°N 130°E on the launch date of KSR-III. Considering the typical spatial variation of the ozone number density profiles, they are considered to be reasonable for the purposes of comparison. Note that ozone is mainly produced in equatorial region where atomic oxygen, the most important source for ozone is abundant due to stronger solar UV radiation dissociating molecular oxygen. Then the ozone is transported to higher latitudes, which results

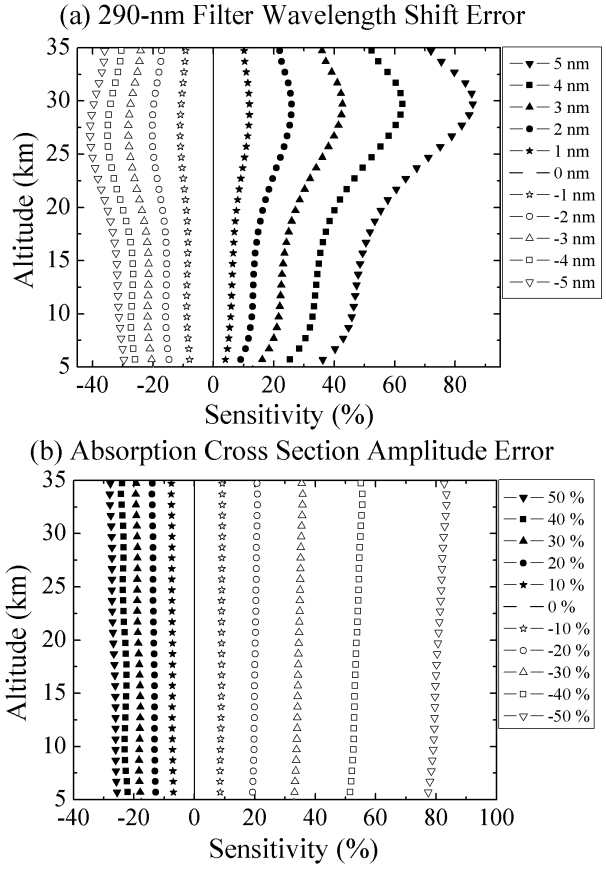

Fig. 7. Profile sensitivity due to errors in the wavelength shifts of the filter response function and the absorption cross-section amplitude.

in a latitudinal distribution of ozone, in general. The density change of ozone from the equator to the poles is at most a factor of two, which is much smaller than the vertical variation. Seasonally, total ozone density reaches its maximum in spring and minimum in autumn due to a strength change of the equator-to-pole transport mechanism in the stratosphere, the so-called Brewer-Dobson circulation (See Ref. 25 for a detailed description of the seasonal change and the global distribution.)

There are various random error sources in our measurement due to the calibration, the telemetry system and electronics, the rocket altitude obtained from radar tracking, and the retrieval algorithm parameters. The calibration error was estimated to be less than 1.2 % in Section IV. The radar tracking has a 20-m error causing less than a 1 % error on the ozone number density above 15 km. A total errors of 15 % is estimated for altitudes below 20 km, 7 % for the altitude range between 20 and 25 km, and 15 % for above 25 km for this flight.

Among the parameters in the retrieval algorithm, the errors in characterizing wavelengths to measure the interference filter response function and the absorption cross section are found to be the most significant sources of error for the ozone number density profiles. Figure 7 shows the profile sensitivity due to errors in the wavelength shifts for the 290-nm filter response function from -5 nm to $+5$ nm range in 1-nm step and in the amplitude for absorption cross section from -50 % to $+50$ % in 10 % steps. The +5-nm shift in filter response function contributes an $\sim$80 % increase to the profile at about 30 km, but in the case of +50 % errors in absorption cross section amplitude, the profile is reduced by about 30 %. These can be explained with the absorption characteristics of ozone at the altitudes considered in the stratosphere. The profile is found to be more sensitive by positive wavelength shifts than to negative wavelength shifts in the filter response function, but in case of errors in the absorption cross section amplitude, the profile is more sensitive to negative errors. Note that the ozone absorption cross section peaks near 255 nm and decreases with wavelengths for wavelengths greater than 255 nm, and the cross section is included in the exponential term in Eq. (3) with a negative sign in the exponent. Note also that the detector's response function is out of the exponential term in the same equation with positive signs.

VI. SUMMARY

In this paper, the development, the calibration, and the flight tests of a radiometer applicable with the sounding rocket KSR-III were presented with detail descriptions of the calibration, the data retrieval algorithm and the error analysis. The radiometer consists of a quartz lens, interference filters, phototubes, and electronic circuits. Four-channel radiometers were onboard KSR-III: 255, 290, and 310-nm channels for UV measurements and 450-nm visible channels for the correction of the rocket attitude change. The calibration system mainly consisted of a monochromator, light sources, detectors, an OPM, a control PC, and data acquisition software. With the calibration of each interference filter, the light intensity response function for each filter was successfully obtained and the center wavelength shift was confirmed to have a tendency to move toward shorter wavelength as the angle of incidence increased. The angular response of the integrated radiometer was also measured. The flight test of the radiometer onboard the KSR-III was carried out on Nov. 28, 2002, to measure the UV intensity and to transmit the data to the ground station in real time during the flight. The data reduction algorithm provided the ozone number density which was calculated numerically by using the calibration results and the measured flight data. Our result, in general, shows reasonable agreement with other measurements in the lower stratosphere.

ACKNOWLEDGMENTS

The authors express their appreciation to all members of the staffs that participated in the development and flight tests of KSR-III and to the Korea Meteorological Administration for the ozonesonde data at Pohang. In particular, we would like to thank Prof. T. Watanabe at Tsukuba College of Technology for advice on the sensor calibration. This sounding rocket research program was supported by the Ministry of Science and Technology, the Republic of Korea. The analysis work was supported by the Yonsei University Research Fund for 2003.

REFERENCES

[1] F. Makino, Adv. Space Res. **30**, 1095 (2002).
[2] I. Sadourny, Adv. Space Res. **30**, 1105 (2002).
[3] J. R. Pardo, L. Pagani, G. Olofsson, P. Febvre and J. Tauber, J. Quant. Spectrosc. Radiat. Transfer **67**, 169 (2000).
[4] H. Vömel, S. J. Oltmans, B. J. Johnson, F. Hasebe, M. Shiotani, M. Fujiwara, N. Nishi, M. Agama, J. Cornejo, F. Paredes and H. Enriquez, J. Geophys. Res. **107**, 10.1029/2001JD000707 (2002).
[5] A. J. Krueger, Ph.D. Dissertation, Colorado State Univ., Fort Collins (1984).
[6] T. Watanabe, I. Naito and T. Ogawa, J. Geomag. Geoelectr. **44**, 1057 (1992).
[7] J. P. Burrows, M. Webwer, M. Buchwitz, V. V. Rozanov, A. L. Weissenmayer, A. Richer, R. de Beek, R. Hoogen, K. Bramstedt, K. U. Eichmann, M. Eisinger and D. Perner, J. Atm. Sci. **56**, 151 (1999).
[8] C. Brogniez, A. Bazureau, J. Lenoble and W. P. Chu, J. Geophys. Res. **107**, 4758 (2002).
[9] R. L. Lucke, D. R. Korwan, R. M. Bevilacqua, J. S. Hornstein, E. P. Shettle, D. T. Chen, M. Daehler, J. D. Lumpe, M. D. Fromm, D. Debrestian, B. Neff, M. Squire, G. König-Langlo, J. Davies, J. Geophys. Res. **104**, 18785 (1999).
[10] J. L. Bertaux, G. Mégie, T. Widemann, E. Chassefière, R. Pellinen, E. Kyrola, S. Korpela and P. Simon, Adv. Space Res. **11**, 237 (1991).
[11] J. D. Mill, R. R. O'Neil, S. Price, G. J. Romick, O. M. Uy and E. M. Gaposchkin, J. Spacecraft and Rockets **31**, 900 (1994).
[12] J. Kim, C. J. Park, K. Y. Lee, D. H. Lee, H. K. Cho, Y. O. Kim, G. R. Cho and J. H. Park, J. Geophys. Res. **102**, 16123 (1997).
[13] J. Kim, S. J. Lee, J. D. Lee, G. R. Cho, Y. I. Won and H. K. Cho, Adv. Space Res. **27**, 2025 (2001).
[14] A. C. Holland, R. A. Barnes and H. S. Lee, Appl. Opt. **24**, 3288 (1985).
[15] K. Y. Lee, D. H. Lee, J. Kim, C. J. Park and H. K. Cho, J. Astron. Space Sci. **11**, 53 (1994).
[16] S. H. Hwang, J. Kim, Y. D. Chun, Y. H. Kim and M. H. Jang, Aerospace Engineering and Technology **2**, 83 (2002).
[17] S. W. Kim, S. J. Lee and J. D. Lee, J. Kor. Soc. for Aeronaut. and Space Sci. **29**, 137 (2001).
[18] Oriel instruments, *The book of photon tools* (Oriel Instruments, Connecticut, 2000), p. 10.
[19] Newport, *Optics and Mechanics 1999-2000* (Newport, California, 2000), p. 12.
[20] Hamamastu, *Phototubes* (Hamamastu, Shizuoka-ken, Japan, 1996).
[21] J. E. Mentall, J. E. Frederick and J. R. Herman, J. Geophys. Res. **86**, 9881 (1981).
[22] M. P. Thekaekara, Appl. Opt. **13**, 518 (1974).
[23] L. T. Molina and M. J. Molina, J. Geophys. Res. **91**, 14501 (1986).
[24] World Meteorological Organization(WMO), Atmospheric ozone 1985-assessment of our understanding of the processes controlling its present distribution and change, WMO Rep. 16, p. 300, Washington DC (1986).
[25] H.-K. Cho, J. Kim, S. N. Oh, S.-K. Kim, S.-K. Baek and Y. G. Lee, Korean J. of Atmos. Sci. **6**, 97 (2003).